

Silver nanostructure sensing platform for maximum-contrast fluorescence cell imaging

Kyung-Min Lee
Arup Neogi
Purnima Basu Neogi
Minjung Kim
Bongsoo Kim
Rafal Luchowski
Zygmunt Gryczynski
Nils Calander
Tae-Youl Choi

Silver nanostructure sensing platform for maximum-contrast fluorescence cell imaging

Kyung-Min Lee,^a Arup Neogi,^a Purnima Basu Neogi,^b Minjung Kim,^c Bongsoo Kim,^c Rafal Luchowski,^d Zygmunt Gryczynski,^d Nils Calander,^e and Tae-Youl Choi^f

^aUniversity of North Texas, Department of Physics, Denton, Texas 76203

^bUniversity of North Texas, Department of Biology, Denton, Texas 76203

^cDepartment of Chemistry, KAIST, Deajeon, 305-701, Korea

^dUniversity of North Texas Health Science Center, Department of Molecular Biology and Immunology Fort Worth, Texas 76107

^eMacquarie University, Department of Physics, NSW 2109, Sydney, Australia

^fUniversity of North Texas, Department of Mechanical and Energy Engineering, Denton, Texas 76207

Abstract. We present herein a silver nanostructure-assisted sensing platform which consists of a combined structure of Ag nanowire (NW) and nanodot (ND) array. Highly enhanced fluorescence from fluorophore is attributed to a strongly coupled optical near-field interaction between proximately located Ag NW and NDs. We obtained enhanced fluorescence intensity with up to 140 folds, as contrasted from background intensity, reaching a theoretical maximum value. On the other hand, fluorescence lifetime was greatly reduced to 0.27 ns (from 2.17 ns for the same fluorophores without nanostructure). This novel platform can be a promising utility for optical imaging and labeling of biological systems with a great sensitivity. © 2011 Society of Photo-Optical Instrumentation Engineers (SPIE). [DOI: 10.1117/1.3579157]

Keywords: Ag nanowire; nanodot; focused ion beam; fluorescence; cell imaging.

Paper 10555R received Oct. 12, 2010; revised manuscript received Mar. 6, 2011; accepted for publication Mar. 25, 2011; published online May 10, 2011.

1 Introduction

Applications of fluorophore–metal interactions such as metal-enhanced fluorescence (MEF) have been actively sought through theoretical development since the 1980s. The presence of metallic surfaces or particles in the proximity of fluorophores can dramatically change spectral properties of fluorophores.^{1–6} Additionally, recent active research in the use of nanostructures has enabled favorable modification of photophysical spectroscopies of biological systems.

A noble metal such as silver (Ag) or gold (Au) has been used as a substrate for MEF imaging. Recently MEF has shown a dramatically increased fluorescence emission while reducing lifetime, which leads to decreased photobleaching.⁷ Also, Ag or Au has a large scattering and absorption cross section in its nanostructure formation. Such enhanced cross sections can offer highly sensitive and contrasted imaging.⁸ In addition, a collective free electron oscillation, known as surface plasmon, on Ag or Au surface can be tuned to be activated in the near-infrared (NIR) region. Therefore, nanorods or nanoshells that are triggered by an NIR light source have been used for imaging as well as for therapy of *in vivo* tissues utilizing a large penetration depth of NIR through tissues.^{9,10} In this manuscript, we introduce a novel nanostructure platform using the near-field interaction, which leads to a highly enhanced fluorescence image. For fluorophore, we used LDS798 dye {1-ethyl-4-[4-(p-dimethylaminophenyl)-1,3-butadienyl]-quinolinium Perchlorate} dissolved in 0.2% poly(vinyl) alcohol (PVA) (abbreviated as LDS798-PVA). While MEF is induced by optical

interaction between a metal structure and dielectric material such as a cell or fluorophore, this novel platform, which integrates Ag nanowire (NW) and nanodot (ND) array (NW-NDA), provides resonantly enhanced optical coupling between the two metal nanostructures. Hence, a much higher intensity of fluorescence in this structure than in a metal-dielectric interface is expected. Employing this novel platform, NW-NDA, we have detected remarkably enhanced fluorescence of LDS798-PVA. A strongly localized field was induced on the surface of Ag ND by light irradiation due to a “lightening rod effect.”^{2,11,12} Highly localized optical coupling between NW and ND arrays occurred when Ag NW was proximately located to the arrayed NDs. Since the optical coupling between the NW and NDs would increase the density of the optical mode, this would lead to higher radiation pumping and decaying rates.

2 Methods and Material

2.1 Preparation of the Measurement Platform

We used a glass substrate for backside illumination of excitation light (635 nm). A Ag thin film (50-nm thick) was deposited on top of the glass by sputtering. A focused ion beam (FIB-FEI Nova 200 Nanolab) was utilized to create a nanodot array by ion beam milling at 30 kV/30 pA. Each nanodot is 100 to 200 nm in diameter and 50 nm in height. The array size was $8 \times 5 \mu\text{m}^2$, which is comparable to a typical cell dimension. A single Ag NW was placed in the proximity of the ND array with an aid of a nanomanipulator (Omniprobe Autoprobe 200, Dallas, Texas).

Address all correspondence to: Tae-Youl Choi, University of North Texas, Department of Mechanical and Energy Engineering, Denton, Texas 76203; Tel: 940-565-2198; Fax: 940-369-8675; E-mail: choi@egw.unt.edu

2.2 Ag NW Growth

Ag NWs were synthesized in a horizontal hot-wall single-zone furnace. The Ag slug (99.99%, Sigma-Aldrich) was placed in an alumina boat at the center of a heating zone and a c-cut sapphire substrate was placed at a few centimeters downstream from the center of the heating zone. Ar gas flowed at a rate of 100 sccm, maintaining the chamber pressure at 10 Torr. Ag slug was heated at 780 °C and the Ag vapor was transported to the lower temperature region by carrier gas, where Ag NWs were grown on the substrate. The temperature of the substrate was maintained at 730 °C. Readers can refer to the earlier report for more detailed information.¹³

2.3 Placement of a Single Ag NW

A single Ag NW was transferred from the substrate (SiO₂) to the prepatterned Ag ND array using the nanomanipulator. The transferring method is the same as in the previous report.¹⁴ However, in this study, the electron beam-induced Pt (EB-Pt) deposition for adhesion between the Ag NW and nanomanipulator was not necessary. Since one end of the NW was freestanding and the other end was loosely bounded to the substrate, we only needed a mechanical force from the nanomanipulator in the translational direction, which is enough to overcome the bonding potential between the NW and substrate. We lifted up the nanomanipulator rapidly in the vertical direction in order to pull out the NW. Transferring the NW to the prepatterned structure and placing it in the ND array were sequentially completed. In placing the NW inside the array, mechanical rotation and pressure was needed on the nanomanipulator for a correct direction and secure placement of the NW. In contrast to the previously reported NW deposition, no ion-beam cut separating the nanowire and the nanomanipulator was needed because the EB-Pt deposition was not performed. Figure 1 shows the schematic view and scanning electron microscope (SEM) image of NW-NDA. To clarify dependency of the gap between NW and ND on the field enhancement, the NDs array was fabricated with variable vertical gaps.

2.4 Experimental Setup

A thin layer of LDS798-doped PVA was prepared by spin-coating on the glass surface with previously deposited nanowire. We used a spin-coating system (Model P6700 series, Special Coating Systems, Inc., Indianapolis, Indiana) at 3000 rpm for 100 s. For intensity and time-resolved measurements a confocal system MicroTime200 (PicoQuant, GmbH, Berlin, Germany) has been used. The detection part equipped with a microphoton device detector, type PD1CTC, has been integrated with an Olympus IX71 inverted microscope. An excitation source was provided by a LDH-P-C-635B pulsed laser diode at 635 nm and was spectrally precleaned by a band-pass filter (z636/10×, Chroma Technology Corp., Bellows Falls, Vermont). A sample composed of NWs and NDs deposited on a glass cover slip with a layer of spin-coated LDS798-PVA was mounted on a microscope stage in an upside down configuration. A water immersion objective lens (Olympus 60×, 1.2 NA UPlanSApo, Tokyo, Japan) was used to focus excitation light on the sample. The same objective lens collected the

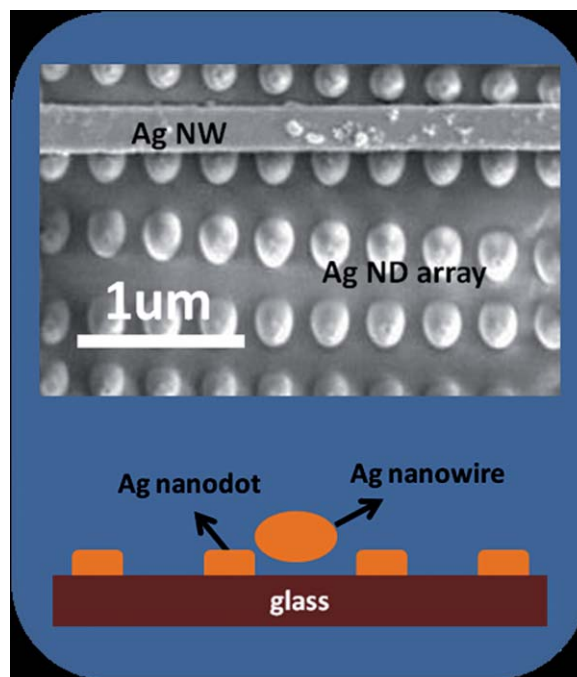


Fig. 1 Schematic view and SEM image of NW-NDA for a fluorescence imaging platform.

fluorescence photons after laser pulses that were synchronized with the PicoHarp 300 time-correlated single-photon counting module. Fluorescence emission was separated from scattered light by using a combination of 640-nm razor edge and 650-nm long-wavelength pass filters (Semrock). The data analysis of fluorescence decay was performed using the SymPhoTime (v. 5.0) software package, that also controlled the data acquisition. The fluorescence decay curves were analyzed by means of iterative deconvolution with the same software program. A sum of exponentials was found,

$$I(t) = \sum_i \alpha_i \exp(-t/\tau_i),$$

where α_i and τ_i are pre-exponential factors and fluorescence lifetimes, respectively.

3 Results and Discussion

Figure 2 shows the fluorescence intensity and lifetime measurement images. Along the NW in the inset, bright fluorescence at proximate region between NW and NDA is indicated. Initially, we fabricated the NDA with various gaps from the NW in order to clearly see the gap dependency of field enhancement. The localized enhancement of the field might be attributed to the optical coupling between the localized field in the NDA and in the NW. The former can be described as a highly dense optical field line at the edge-shaped geometry (in our case, highly confined corner of cylindrical interface). Since two structures are close to each other, in the near field regime, the optical coupling between two metallic systems concentrates a local electrical field on the fluorophore so that the highly elaborated radiation decay rate is expected. In addition, the excited state of the fluorophore remained for a short time as additional photonic modes were

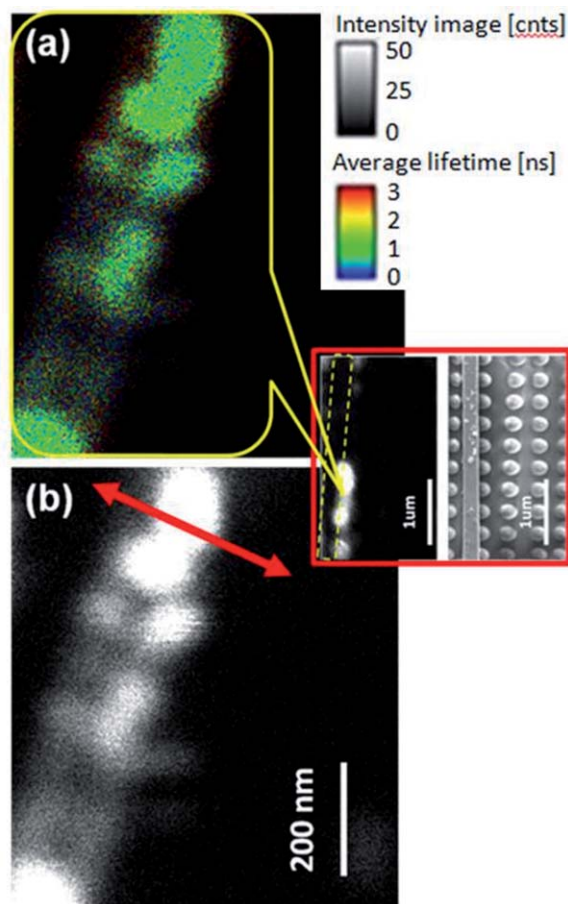


Fig. 2 Fluorescence intensity and lifetime image of LDS798-PVA deposited on NW-NDA: (a) Magnified images for lifetime and (b) fluorescence intensity of the indicated area from the inset. Dashed line in the inset is the Ag NW. Double headed arrow is a region for analysis, which is shown in Fig. 4. At the sites where NW and ND are closely located (right bottom and right and left top in Ag NW), enhanced fluorescence intensities are shown.

introduced by the resonantly coupled field, which in turn decreased lifetime.¹⁵ This gave rise to shorter lifetime of 0.27 ns and brighter fluorescent emission of up to 140 folds, as compared to the measurement without the NW-NDA-based platform that was used for background (control) intensity in the current study.

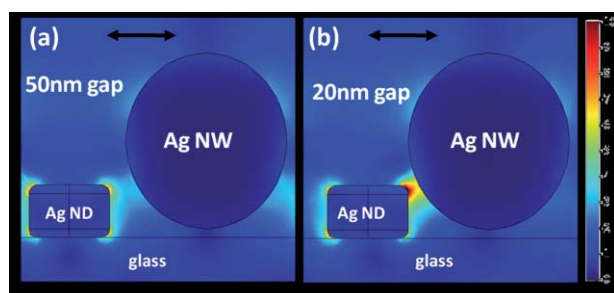


Fig. 3 Simulated result for the local electric field distribution for NW-NDA. Incident light was polarized perpendicularly to the NW. The gap between Ag NW and ND array was assigned to be 50 nm in (a) and 20 nm in (b), respectively. Fairly enhanced field distribution between the NW and ND array was shown in smaller gap (20 nm).

In order to confirm the change in lifetime and increase of fluorescence emission, a theoretical simulation was conducted using the finite element method. A program package, COMSOL 3.5a with the RF module on a Linux computer cluster with 15 nodes (each node having 18 GBytes of internal memory), was used for this simulation. The program solves the finite difference time domain electric fields based on the full set of Maxwell's equations by assigning each domain (e.g., Ag NW, Ag ND, glass, air) optical properties such as refractive indices with input intensity field of 635 nm. Figure 3 shows the simulation result for the same structure of the experiment without the fluorophore. Therefore, Fig. 3 shows only the field enhancement due to ND-NW construct. In Fig. 3(a), no enhanced field distribution in the gap of Ag NW and ND was found when they are separated by larger than 20 nm. However, an enhanced field was detected at 20 nm of the gap between the NW and ND as shown in Fig. 3(b). This field enhancement can be understood by the lightning rod effect. A quasi-electrostatic condensing of electric field lines at a highly confined volume of arbitrary geometry can give rise to a magnificently localized field. As long as the effective curvature of the highly confined volume is much smaller than the wavelength of light, this effect is more prominent. And when Ag NW is proximately located to the arrayed NDs, highly localized optical coupling between the NW and ND array would occur since many free electrons in an Ag NW would be responsible for coulombic interaction with the localized field on NDA. Thus, an increase in the emission intensity is expected as a result of optical coupling that increases the local incident field on the fluorophore. This will lead to higher radiation pumping and decaying rates and subsequently produce enhanced fluorescence intensity and reduced me.

Figure 4(a) shows the enhanced fluorescence intensity at the double-headed arrow region in Fig. 2(b). It showed 140-fold increased intensity as compared to that of the control (background). A similar enhancement factor was theoretically obtained with a maximum value due to the lightning rod effect.¹ In Fig. 4(b), a schematic view was used to explain that the enhanced fluorescence intensity was caused by the field enhancement at the proximate sites in NW-NDA. The proximation dependency of field enhancement was confirmed by our experimental and

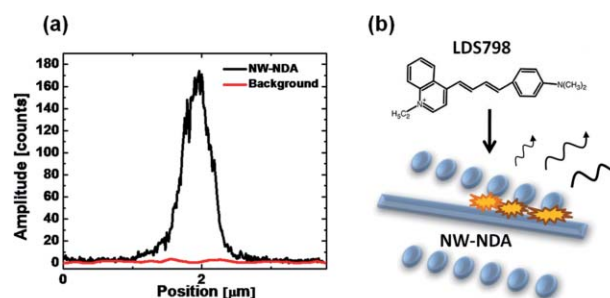


Fig. 4 (a) Fluorescence intensity comparison of LDS 798-PVA on NW-NDA between the field enhanced region (double headed arrow in Fig. 2) and background. 140-fold increased intensity from the background was revealed, which is close to a maximum theoretically predicted value; (b) highly enhanced fluorescence intensity due to field enhancement at proximate sites was shown schematically.

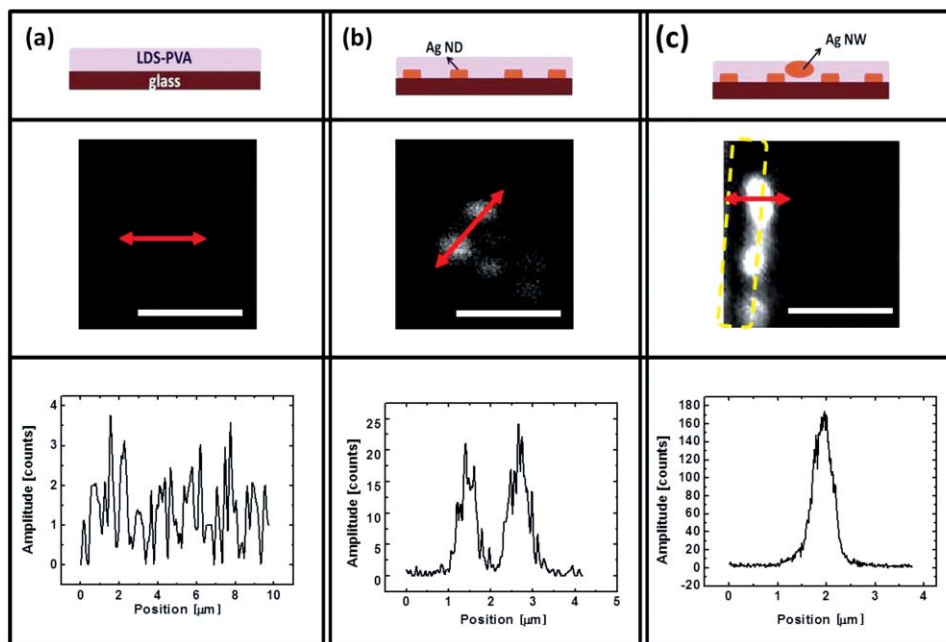


Fig. 5 Fluorescence intensity studies for three different types: (a) LDS-PVA alone, (b) LDS-PVA with Ag NDs, and (c) LDS-PVA with Ag NDs and NW on glass. Red double-headed arrows indicate scanning cross sections for spatial distributions of fluorescence intensity. White bars on the fluorescence images indicate 1-μm scales.

simulated results as shown in Figs. 2 and 3. Therefore, we conclude that the large enhancement of fluorescence intensity is attributable to high quantum yield from optical coupling between Ag NW and NDA. In Fig. 5, three different imaging systems such as LDS-PVA alone, LDS-PVA on Ag NDA, and LDS-PVA on Ag NDA and NW for fluorescence intensity measurement are shown for clear comparison with their schematics and spatial intensities. In Fig. 5(b), two bright spots are fluorescence from two proximate NDs. Due to MEF from two Ag NDs, fluorescence was fairly increased from the structure with

fluorophore alone [Fig. 5(a)]. On the other hand, highest intensity was found on the NW-NDA [Fig. 5(c)].

Decay of measured fluorescence intensity is presented in Fig. 6. A fitting parameter for fluorescence decay of the LDS 798 was obtained using a single exponential (χ^2) value equal to 1.347. Analysis of intensity decay revealed a single fluorescence lifetime of 0.27 ns. The fluorescence lifetime drops significantly from 2.17 ns (dashed line in the graph) which has been reported previously for the same material.¹⁶ This quenched lifetime can be explained by modifying the total radiative decay rate ($\Gamma_{total} = \Gamma + \Gamma_{NW-NDA}$) incorporating the NW-NDA-induced

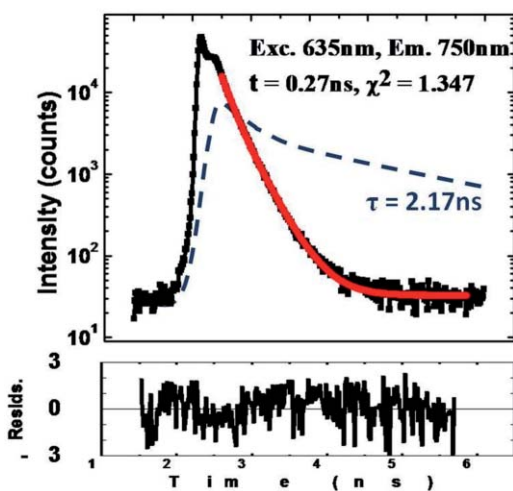


Fig. 6 Fluorescence intensity decay of LDS 798-PVA on NW-NDA. Excitation was 635 nm. The fitting result for fluorescence lifetime was 0.27 ns. The dashed line and lifetime of 2.17 ns are the decay line for Ag thin film without NW-NDA arrangement.

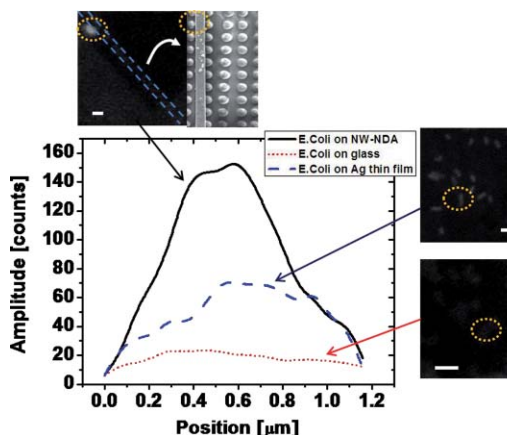


Fig. 7 Fluorescence image of E. coli placed on the three different structures such as NW-NDA, Ag thin film (60-nm thickness), and glass. The most clear image of E. coli with highest fluorescence intensity was obtained from the NW-NDA arrangement. Actual locations of NW and E. coli are indicated by dotted lines and circles.

radiative decay rate, $\Gamma_{\text{NW-NDA}}$, in addition to normal radiative decay rate, Γ . It should be clarified that the first fast component is due to the small amount of post-pulse after a main excitation pulse.

Based on our results in this paper, we envision that NW-NDA can function as a surface-enhanced fluorescence-active platform where very high fluorescence signal enhancement is expected. With this token, *E. coli* (*Escherichia coli*) was used to demonstrate our technology for biological imaging applications. *E. coli*-suspended solutions of 1 μl were dropped on glass, Ag thin film (60-nm thickness), and NW-NDA. After the solutions were totally dried, DAPI (4',6-diamidino-2-phenylindole) was used to stain each sample. DAPI is commonly used for staining DNA inside a cell as a fluorescent dye. Since *E. coli* is relatively small in size in our experiment (1 to 2 μm), DAPI can work for imaging the whole topological feature of *E. coli*. The Zeiss Axiovert 200 M confocal optical microscope with 405-nm excitation was used to image *E. coli*. Figure 7 shows the images of *E. coli* on glass, Ag thin film, and NW-NDA with their fluorescence intensities. *E. coli* for measuring fluorescence intensity is marked by the yellow dotted circles on fluorescence image. The scale bar on each image corresponds to 1 μm . SEM image of NW-NDA and marked location of *E. coli* on it are shown next to the NW-NDA fluorescence image. A blue dotted line on the fluorescence image was drawn to indicate the location of NW. It is clearly found that the brightest image, hence highest fluorescence intensity is obtained from NW-NDA. Our observation on greatly enhanced field in the Ag nanostructure-assisted (NW-NDA) sensing platform could be extended to monitor exocytotic activities occurring at the surface of a cell membrane due to the surface-enhanced near-field interaction.¹⁷ Thus, in the vicinity of a cell membrane in contact with the enhanced field, the exocytotic events and vesicle release to the extracellular space can be indicated by great sensitivity with high fluorescence signal amplification.

4 Conclusion

A nanostructure platform composed of a Ag NW and ND array was fabricated by using a nanolithography approach. We took a fluorescence image and measured a fluorescence lifetime for fluorophore on this platform. The enhanced fluorescence agreed well with a simulation result. We confirmed that the enhanced fluorescence was indeed due to the near field optical interaction, mediated by optical coupling between Ag NW and NDs. An array of NDs and proximately located NW induced a fairly enhanced field of up to 140 folds along the NW, as contrasted from background intensity. This result is close to a maximum value predicted theoretically using a lightning rod effect. When the incident light irradiates from the bottom of a glass substrate, an enhanced field due to the coupled near-field interaction leads to a brighter fluorescence image, giving rise to shortened lifetime, with a great sensitivity. This novel nanoengineered platform opens up a new horizon for a more efficient and direct way to image a cell and biological system. The proposed instrument can provide a non-invasive approach for studying membrane-proximal molecular events in cancer cells, which may lead to a clue for diagnosis of cancer.

Acknowledgments

This project was supported by National Science Foundation (CMMI-0841265) and partially supported by the Center for Nanoscale Mechatronics and Manufacturing of the 21st Century Frontier Research Program. The authors thank the Center for Advanced Research and Technology (CART) at the University of North Texas for supporting this research.

References

1. J. Kummerlen, A. Leitner, H. Brunner, F. R. Aussenegg, and A. Wokaun, "Enhanced dye fluorescence over silver island films – analysis of the distance dependence," *Mol. Phys.* **80**(5), 1031–1046 (1993).
2. K. Sokolov, G. Chumanov, and T. M. Cotton, "Enhancement of molecular fluorescence near the surface of colloidal metal films," *Anal. Chem.* **70**(18), 3898–3905 (1998).
3. J. R. Lakowicz, "radiative decay engineering: biophysical and biomedical applications," *Anal. Biochem.* **298**, 1–24 (2001).
4. J. R. Lakowicz, Y. Shen, S. D' Auria, J. Malicka, J. Fang, Z. Gryczynski, and I. Gryczynski, "Radiative decay engineering: 2. effects of silver island films on fluorescence intensity, lifetimes, and resonance energy transfer," *Anal. Biochem.* **301**, 261–277 (2002).
5. J. DeSaja-Gonzalez, R. Aroca, Y. Nagao, and J. A. DeSaja, "Surface enhanced fluorescence and Raman spectra of N-Octadecyl-3,4:9,10-perylene-tetracarboxylic monoanhydride on silver islands," *Spectrochim. Acta Part A* **53**, 173–181 (1997).
6. T. Schalkhammer, F. R. Aussenegg, A. Leitner, H. Brunner, G. Hawa, C. Lobmaier, and F. Pittner, "Detection of fluorophore-labelled antibodies by surface-enhanced fluorescence on metal nanoislands," *Proc SPIE* **2976**, 129–136 (1997).
7. E. Matveeva, Z. Gryczynski, J. Malicka, I. Gryczynski, and J. R. Lakowicz, "Metal-enhanced fluorescence immunoassays using total internal reflection and silver island-coated surfaces," *Anal. Biochem.* **334**, 303–311 (2004).
8. K. Sokolov, M. Follen, J. Aaron, I. Pavlova, A. Malpica, R. Lotan, and R. Richards-Kortum, "Real-time vital optical imaging of precancer using anti-epidermal growth factor receptor antibodies conjugated to gold nanoparticles," *Cancer Res.* **63**, 1999–2004 (2003).
9. P. K. Jain, X. Huang, I. H. El-Sayed, and M. A. El-Sayed, "Noble metals on the nanoscale: optical and photothermal properties and some applications in imaging, sensing, biology, and medicine," *Acc. Chem. Res.* **41**(12), 1578–1586 (2008).
10. X. Huang, I. H. El-Sayed, W. Qian, and M. A. El-Sayed, "Cancer cell imaging and photothermal therapy in the near-infrared region by using gold nanorods," *J. Am. Chem. Soc.* **128**, 2115–2120 (2006).
11. T. Hayakawa, S. T. Selvan, and M. Nogami, "Field enhancement effect of small Ag particles on the fluorescence from Eu³⁺-doped SiO₂ glass," *Appl. Phys. Lett.* **74**(11), 1513–1515 (1999).
12. S. T. Selvan, T. Hayakawa, and M. Nogami, "Remarkable influence of silver islands on the enhancement of fluorescence from eu³⁺ ion-doped silica gels," *J. Phys. Chem. B.* **103**, 7064–7067 (1999).
13. P. Mohanty, I. Yoon, T. Kang, K. Seo, K. S. K. Varadwaj, W. Choi, Q. Park, J. Ahn, Y. Suh, H. Ihee, and B. Kim, "Simple vapor phase synthesis of single-crystalline Ag NWs and single NW surface-enhanced Raman scattering," *J. Am. Chem. Soc.* **129**, 9576–9577 (2007).
14. K. M. Lee, T. Y. Choi, S. K. Lee, and D. Poulikakos, "Focused ion beam-assisted manipulation of single and double β -SiC nanowires and their thermal conductivity measurements by the four-point-probe $3-\omega$ method," *Nanotechnology* **21**, 125301 (2010).
15. C. D. Geddes and J. R. Lakowicz, "Editorial: Metal-enhanced fluorescence," *J. Fluoresc.* **12**(2), 121–129 (2002).
16. R. Luchowski, P. Sarkar, S. Bharill, G. Laczko, J. Borejdo, Z. Gryczynski, and I. Gryczynski, "Fluorescence polarization standard for near infrared spectroscopy and microscopy," *Appl. Opt.* **47**, 6257–6265 (2008).
17. C. K. Chen, T. F. Heinz, D. Ricard, and Y. R. Shen, "Surface-enhanced second-harmonic generation and Raman scattering," *Phys. Rev. B* **27**(4), 1965–1979 (1983).